Article

Not peer-reviewed version

Confinement of a Styryl Dye into Nanoporous aluminophosphates: Channels vs Cavities

Ainhoa Oliden-Sánchez , Rebeca Sola-Llano , Joaquín Pérez-Pariente , Luis Gómez-Hortigüela * , Virginia Martínez-Martínez *

Posted Date: 12 February 2024

doi: 10.20944/preprints202402.0625.v1

Keywords: styryl dyes; aluminophosphates; photoactive hybrid systems; MgAPO; AEL framework; CHA framework; fluorescence; nanochannels; cavities; molecular sieves

Article

Confinement of a Styryl Dye into Nanoporous aluminophosphates: Channels *vs* Cavities

Ainhoa Oliden-Sánchez [1], Rebeca Sola-Llano [1], Joaquín Pérez-Pariente [2], Luis Gómez-Hortigüela [2,*] and Virginia Martínez-Martínez [1,*]

[1] Departamento de Química Física, Universidad del País Vasco (UPV/EHU), Apartado 644, 4808 Bilbao, Spain; ainhoa.oliden@ehu.eus, rebeca.sola@ehu.eus

[2] Instituto de Catálisis y Petroleoquímica-CSIC, c/ Marie Curie 2, 28049 Cantoblanco, Madrid, Spain; jperez@icp.csic.es

* Correspondence: lhortiguela@icp.csic (LGH) and virginia.martinez@ehu.eus (VMM)

Abstract: Styryl dyes are generally poor fluorescent molecules inherited from their flexible molecular structures. However, their emissive properties can be boosted by restricting their molecular motions. A tight confinement into inorganic molecular sieves is a good strategy to yield highly fluorescent hybrid systems. In this work, two Mg-aluminophosphate zeotypes (AEL framework, a one-dimensional channeled structure with elliptical pores of 6.5 Å x 4.0 Å; and CHA framework, composed by large cavities of 6.7 Å x 10.0 Å connected by 8-ring narrower windows) were selected for the encapsulation of 4-DASPI dye (trans-4-[4-(Dimethylamino)styryl]-1-methylpyridinium iodide). The synthesis and photophysical properties of 4-DASPI styryl dye occluded within these two types of confinements, AEL and CHA, are optimized and analyzed. The resultant hybrid systems display significantly improved photophysical features compared to 4-DASPI in solution. Molecular simulations reveal a tighter confinement of 4-DASPI in the elliptical channels of AEL, whilst a particular orientation is found within the CHA framework, where one 4-DASPI molecule spans along two adjacent cavities. In the latter scenario, each aromatic ring is positioned on these adjacent cavities and the polymethine chain resides within the 8-ring window, being this confinement slightly less tight than for AEL.

Keywords: styryl dyes; aluminophosphates; photoactive hybrid systems; MgAPO; AEL framework; CHA framework; fluorescence; nanochannels; cavities; molecular sieves

1. Introduction

Styryl dyes consist of an electron donor (D) and electron acceptor (A) building block linked together through a π-conjugated system, forming D-π-A architectures [1,2]. In general, they present high absorption capacity in the blue to green region of the visible spectrum and highly red-shifted fluorescence, as the emission takes place from an intramolecular charge-transfer state (ICT), exhibiting rather large Stokes shifts, an important feature to minimize inner-filter effects (reabsorption and reemission) [3–6]. Their strong push-pull character makes them very promising organic molecules for advanced optical applications, including nonlinear optics (NLO), sensing and bioimaging [3,6–12]. However, they are very flexible molecules and require very rigid environments to restrict their molecular motion in order to achieve high fluorescence or lasing efficiency; indeed, rotational motions around the different bonds are responsible for the non-radiative deactivation, such as trans–cis isomerization, or especially the formation of twisted intramolecular charge transfer (TICT) states, which are usually non-fluorescent [13–15].

In this context, confining these molecules into molecular sieves could restrict their molecular motions, reducing internal conversion. Thus, by forcing a rigid planar D-π-A molecule, an efficient ICT can take place without the involvement of large amplitude motions, yielding high fluorescence or even laser efficiency [16–18]. Besides, a preferred orientation within 1D-nanochannels can lead to

 doi:10.20944/preprints202402.0625.v1

a noncentrosymmetric arrangement, and thus to anisotropic behavior, crucial for nonlinear optical applications [19,20]. Therefore, it is essential to provide a tight confinement for the styryl dyes in order to enhance their photophysical properties and boost new features.

In previous works, we demonstrated that the optimum confinement of LDS-722 styryl dye into the 10-ring elliptical channels of the AEL Mg-doped aluminophosphate framework [20] rendered a material with very promising photophysical properties. By simply changing the inorganic framework, we managed to notably improve the quantum yield of the LDS-722 styryl dye, shifting from the large-pore 12-ring channeled AFI framework, featuring cylindrical channels of 7.3 Å in diameter, to the medium-pore 10-ring elliptical channels of 6.5 Å x 4 Å cross-section of the AEL framework [21]. Consistently, in multiple occasions, we have shown that a proper size match between the dye and the host channel dimensions is crucial for achieving efficient hybrid photoactive systems [22–25].

We subsequently considered the possibility of achieving even a tighter confinement of styryl dyes to further improve their photophysical properties. Nevertheless, a further reduction of the pore size from 10-rings as in AEL to 8-rings (small pore) might prevent the occlusion of these styryl dyes due to the relatively bulky end-groups (N, N-dimethylaniline and pyridinium rings) that would prevent their allocation within such small channels. Thus, apparently, the tightest confinement for these molecules employing nanochanneled zeolites would have been reached. However, there are other types of frameworks among zeolite materials whose void volume is constituted by large cavities that are usually connected by smaller windows [26–29]. These cavity-based zeolite systems are potential hosts for styryl-type dyes, which could be eventually confined within these voids, hence imposing significant restrictions on the motion of both organic groups and the entire molecule. This confinement, unlike that occurring within channels with unlimited dimension along the channel, limits motion in all three directions. Consequently, the restricted motion within the cavities holds promise for enhancing the fluorescence properties of guest dyes.

Within this family of zeolite frameworks based on cavities, the chabazite structure (CHA structure code) is one of the most widely known and used [30]. Its lattice consists of a parallel stacking of double six-membered rings (D6R) in ABC sequence order (each letter represents a different position of the six-membered ring around the stacking direction parallel to the *z*-axis), which are linked by 4-membered rings (a schematic representation is shown in Figure 1c). The resulting structure is a three-dimensional system, with cages accessible through eight-membered ring windows with 3.8 Å diameter, opening into large 6.7 Å x 10.0 Å ellipsoidal cavities [31]. Therefore, in this work we analyze and compare the photophysical properties of a styryl dye, 4-DASPI (trans-4-[4-(Dimethylamino)styryl]-1-methylpyridinium iodide), occluded within two types of confinements: within the one-dimensional medium-size pores of AEL channels, and the cavities of the CHA framework (Figure 1). The incorporation of dye molecules into the pores and channels of zeolites is achieved through crystallization inclusion method [32]; notably, the application of this method to host photoactive dye species within the CHA zeolite framework represents a novel approach, as previous studies with dyes have primarily relied on diffusion methods [33,34]. In fact, this is the only plausible method that allows the occlusion of these particular type of dyes, as the diffusion process would be completely impeded by the bulky aromatic end groups and the small-ring windows.

 doi:10.20944/preprints202402.0625.v1

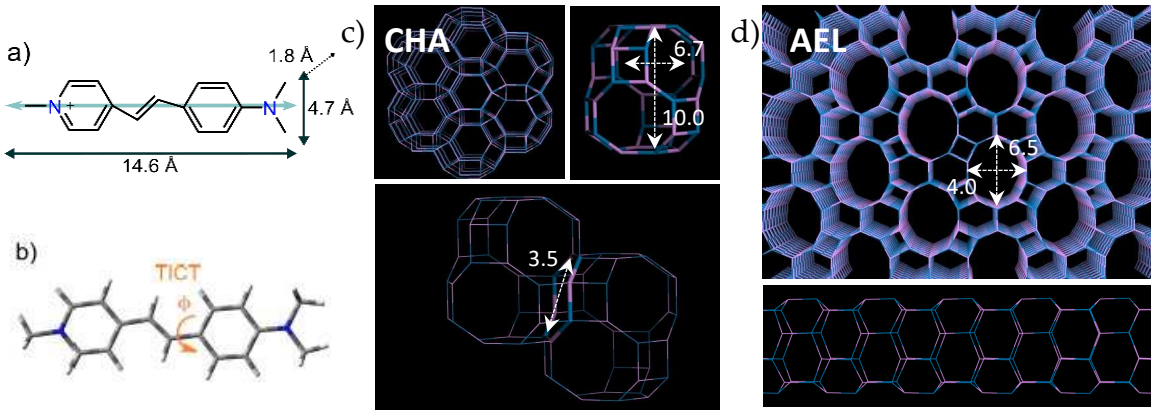

Figure 1. a) Molecular structure, dimensions and transition dipole moment (blue arrow, Mulliken) estimated by theoretical calculations of 4-DASPI dye; b) description of internal twisting through φ as the main deactivation process of electronically excited 4-DASPI [13]. c) 3D cavities of MgAPO-34 (CHA) framework, showing the connection between adjacent cavities (down), and d) 1D channels of MgAPO-11 (AEL) framework.

2. Results and Discussion

2.A. Synthesis of 4-DASPI@MgAPO-CHA System

A dye-free synthesis was first performed to confirm the formation of pure MgAPO-CHA (MgAPO-34 material) under the specified conditions (see Experimental section). Secondly, the dye was incorporated in the synthesis gel (x was set to 0.024), to obtain the dye-loaded 4-DASPI@MgAPO-CHA hybrid system.

PXRD (Figure 2) showed the crystallization of pure CHA materials in both cases, being slightly lower when the material was prepared in the presence of 4-DASPI, suggesting that the dye slightly hindered the crystallization of CHA. The 4-DASPI@MgAPO-CHA solid showed a light orange color, indicating a low presence of dye in the structure. The amount of encapsulated dye estimated was relatively low, of around 0.3 mmol per 100 g of powder sample.

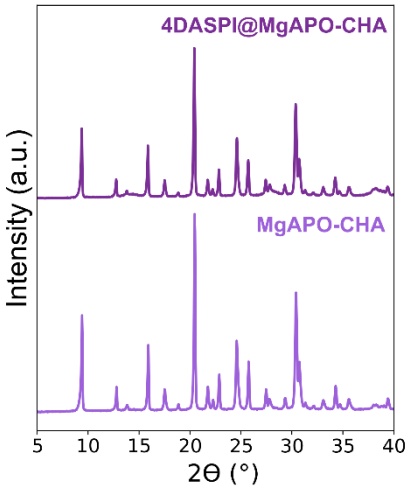

Figure 2. X-ray powder diffractions of CHA samples prepared without (MgAPO-CHA) and with 4-DASPI dye (4-DASPI@MgAPO-CHA).

2.B. Synthesis of 4-DASPI@MgAPO-AEL System

Initially, conditions already used in our previous works were set in order to promote the crystallization of MgAPO-AEL in the presence of 4-DASPI (see Table 1, entries 1 to 4) [20]. However, PXRD patterns showed the concomitant crystallization of the AFI phase in all the conditions tested

 doi:10.20944/preprints202402.0625.v1

(Figure 3), which had not been observed in the absence of the dye. Hence, it is clear that 4-DASPI, as also occurred for LDS 722, acts as an efficient structure-directing agent for the large-pore AFI framework, even if its amount with respect to the organic cation used as template (ethyl-butylamine, EBA) is very small (0.024 dye vs. 1.00 EBA). In fact, by using the same molar gel composition with many other dyes (e.g., Acridine, Methylacridine, Pyronin Y), pure AEL phase was always obtained without any difficulty [24,25,35]. A rough estimation of the relative presence of AEL and AFI phases (by comparing the ratio of the peak intensities corresponding to each phase) showed that the AFI phase was favored at high EBA concentration, i.e., at higher pH values (pH ≈ 5). Thus, in an attempt to minimize the amount of AFI crystallized, we kept the low EBA content (0.75), and reduced the amount of dye (0.008) to minimize its structure-directing effect towards AFI, and we tried two different amounts of phosphoric acid (1.00 and 1.20 P_2O_5, entries 5 and 6 in Table 1) to keep the pH low (pH ≈ 4). Interestingly, in this case we managed to further reduce the AFI concomitant phase to a minimum (entry 6, see Figure 3), although it was not completely prevented (Table 1).

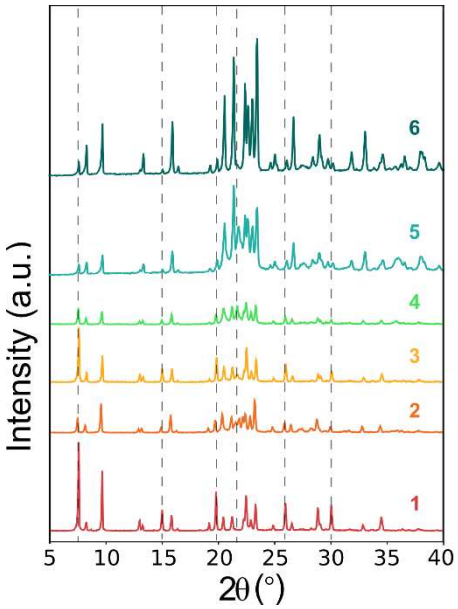

Figure 3. PXRD patterns of 4-DASPI@MgAPO-AEL hybrid systems. Dashed lines denote AFI impurity peaks.

Table 1. Variations in gel composition, final dye uptake (expressed as mmol of dye per 100 g of solid product and as percentage of the dye loaded with respect to the initial amount in the gel), and the final phases achieved (arrows indicate qualitatively the quantity of each phase).

Sample	Gel composition				Dye uptake		X-Ray
4-DASPI@MgAPO-AEL	x (MgO)	y (EBA)	P_2O_5	z (DASPI)	mmol / 100g	%	Phase
1	0.20	1.00	1.00	0.024	8.8	93	AFI(↑)+AEL(↑)
2	0.20	0.75	1.00	0.024	3.1	27	AEL(↑)+AFI(↓)
3	0.10	1.00	1.00	0.024	4.8	41	AFI(↑)+AEL(↑)
4	0.10	0.75	1.00	0.024	3.8	26	AEL(↑)+AFI(↓)
5	0.20	0.75	1.00	0.008	1.7[1]	26	AEL(↑)+AFI(↓↓)+try
6	0.20	0.75	1.20	0.008	2.3	34	AEL(↑)+AFI(↓↓↓)

[1] the lower dye uptake is due to the presence of the dense, non-porous tridymite (try) in the sample.

3.C. Photophysics of 4-DASPI Dye in Solution

In order to better understand the final photophysical properties of the host-guest systems, studies of 4-DASPI in aqueous media are a prerequisite. Table 2 shows the main photophysical

 doi:10.20944/preprints202402.0625.v1

parameters of the 4-DASPI fluorophore in aqueous medium. Briefly, it absorbs in the blue region of the electromagnetic spectrum (λ_{ab} = 449.5 nm) and emits in the red (λ_{fl} = 618.5 nm, Figure S1a). As mentioned above, the large Stokes shift ($\Delta\nu_{st}$ = 6079 cm^{-1}) is due to the push-pull nature of this type of dyes, where fluorescence comes from an intramolecular charge transfer between the donor (dimethylaniline) and acceptor (pyridinium) moieties favored in the excited state (see the difference in the electronic distribution between HOMO and LUMO orbitals in Figure S1b). As expected, the dye shows poor fluorescence features in solution ($\phi_{fl} < 0.01$ and $\tau < 0.1$), being the molecular motions responsible for non-radiative deactivation as the main pathway to the ground state [36,37] (Figure 1b shows the main rotation of 4-DASPI around the single bond between the aniline ring and the pyridylethylene motifs).

Table 2. Photophysical parameters: absorption (λ_{ab}), excitation (λ_{ex}) and fluorescence (λ_{fl}) maximum wavelengths, lifetimes (τ) and fluorescence quantum yields (ϕ_{fl}) of the 4-DASPI fluorophore in different environments (H_2O, MgAPO-CHA and MgAPO-AEL).

4-DASPI@	λ_{ab} (nm)	λ_{fl} (nm)	ϕ_{fl}	τ (ns)
H_2O	329.0[D]/449.5[M]	618.5[a]	< 0.01	<0.01
MgAPO-CHA	343.0[D]/437.0[M]	583.0[a]	0.33	2.73
MgAPO-AEL-1	*	610.0[a]	0.10	0.13 (20%) 3.07 (80%)
MgAPO-AEL-6	*	613.0[a]	0.41	3.30

* Absorption band too broad (deconvolution not possible, Figure S4 and S5). [a] Independent values regardless of excitation wavelength.

However, since these photophysical parameters depend on both the polarity and the viscosity/rigidity of the medium, they can be modulated and significantly improved by freezing this dye within a rigid solid matrix with narrow channels [38]. Consequently, the goal is mainly to limit the flexibility of the molecule by slowing down the molecular motions and TICT in the excited state.

3. Photophysics of 4-DASPI@MgAPO-CHA

Regarding the synthesized dye-doped hybrid materials with CHA framework, Figure 4 shows the occurrence of small MgAPO-34 crystals, with an average dimension of about 1-3 μm. Polarized fluorescence experiments showed that 4-DASPI molecules in MgAPO-34 crystals do not show a preferential orientation (dichroic ratio close to 1). As the analyzer (set before detection) was systematically tuned from 0° to 90° in several steps, the fluorescence signal of particles did not show any intensity dependence, indicating that 4-DASPI molecules are incorporated inside the cages without any preferential orientation.

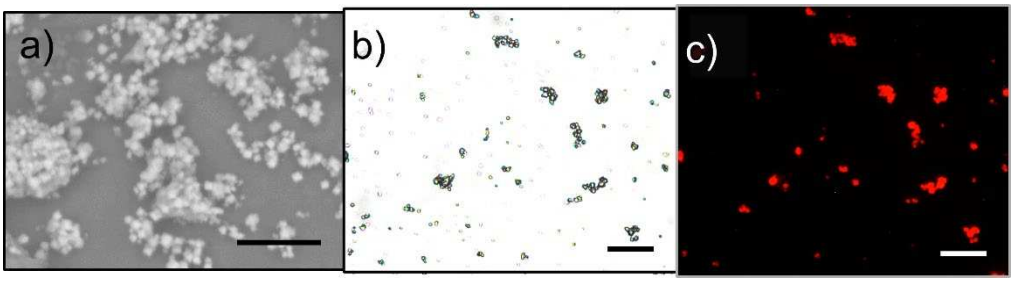

Figure 4. Images taken for 4-DASPI@MgAPO-CHA sample by a) scanning-electron microscopy (SEM) and optical microscopy: b) transmission and b) fluorescence pictures taken under green light excitation (HQ530/30m bandpass). The scale is 20 μm in all of them (black and white bars).

The photophysical characterization of the 4-DASPI@MgAPO-CHA solid sample (Figure 5 and Table 2), reveals two broad absorption bands centered at 343.0 and 437.0 nm. These bands are assigned to the presence of 4-DASPI dye in different protonation forms: dicationic (DC) and

 doi:10.20944/preprints202402.0625.v1

monocationic (MC) species (Figure S2), respectively, as confirmed by the dye photophysics in solution at different pHs, indicating that 4-DASPI is incorporated in both protonation states within the CHA framework (Figure 5a). On the contrary, the fluorescence band centered at 583.0 nm is assigned to the CT state of the MC species, being the emission of DC practically negligible (both in solution and in CHA). This band is blue-shifted with respect to 4-DASPI in water (618.5 nm), a typical effect for chromophores encapsulated in very rigid media. The high Stokes shift ($\Delta\nu_{st}$ = 5416 cm^{-1}) in chabazite, although slightly lower than in solution ($\Delta\nu_{st}$ = 6079 cm^{-1}), together with the bathochromically shifted band registered in the excitation spectrum (maximum at 525 nm, Figure 5b), with respect to its original absorption at 437.0 nm, confirms the charge transfer nature from MC as the main responsible for the fluorescence emission.

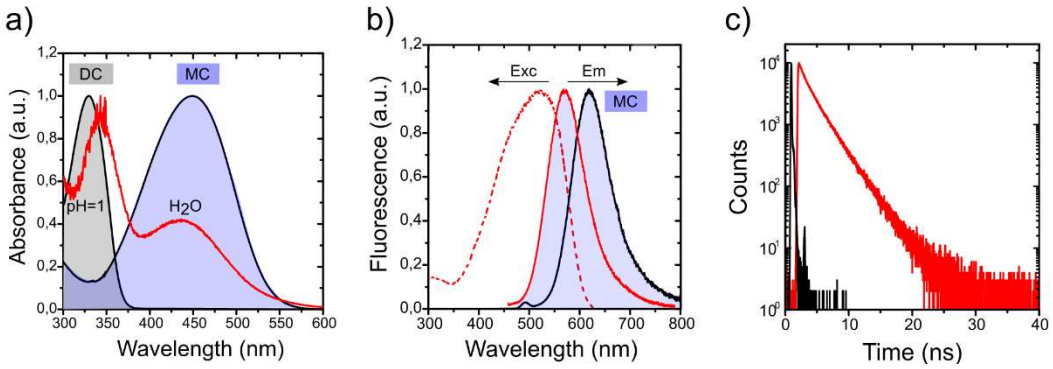

Figure 5. a) Height normalized absorption for 4-DASPI@MgAPO-CHA sample (red) and DASPI in aqueous solution (black), (absorption band of diprotonated 4-DASPI at acidic pH =1 is also included), b) height normalized fluorescence for 4-DASPI@MgAPO-CHA sample (red) and DASPI in aqueous solution (black) at λ_{exc} = 450 nm and λ_{exc} = 420 nm, respectively, and c) fluorescence decay curves recorded for 4-DASPI (aq, black) and for (4-DASPI@MgAPO-CHA powder sample (red).

Is noteworthy at this point that the 4-DASPI dye loaded into CHA material is highly fluorescent regardless of the excitation wavelength, reaching a quantum yield of around 33% (over 30 times higher than in solution), leading also to a greatly enlarged decay lifetime of 2.7 ns, much longer than those obtained in solution (< 0.1 ns), (Table 2), indicating the substantial confinement and motion restriction imposed by the CHA framework on the occluded dye.

3.D. Photophysics of 4-DASPI@MgAPO-AEL

Remarkably, a large amount of dye is occluded into the AEL rich-samples, giving values from 2 to 9 mmol per 100 g of sample powder (Table 1), which represent a percentage from 25 to almost 95% of the dye initially added to the gel, resulting in a very intense orange-reddish powder (Figure S3), rendering very broad absorption bands (Figure S4 and S5). The broadening of the absorption band is a consequence of the great stabilization of the CT state in the ground state, overlapping with the absorption band of the Locally excited "LE" of 4-DASPI. Note here that the presence of the MgAPO-5 (AFI) phase affects the final dye-uptake values, overestimating the amount occluded in AEL. That is, the higher the presence of AFI, the higher the loading of the 4-DASPI dye obtained (note that quantification is performed on bulk powder sample, where it is not possible to distinguish between phases, see Materials and Methods section) (Table 1). This fact may be closely related to the dimensions of the channel of the two unidirectional structures formed in the synthesis procedure, where the wider and more cylindrical 7.3 Å channels of AFI facilitate the incorporation of more 4-DASPI molecules compared to the elliptical and narrower channels of AEL (4.0 Å x 6.5 Å) where confinement is tighter. The presence of AFI impurities not only affects the dye loading but also the overall emission properties of the samples. For instance, sample 1, characterized by the highest amount of AFI, exhibits an overall fluorescence yield of 10%, while this value increases to 41% in sample 6, with the lowest presence of this undesirable phase (Table 2). This fact is again related to the

 doi:10.20944/preprints202402.0625.v1

larger pores of the AFI structure, whose dimensions are too wide to boost the photophysical properties of the dye. This statement is confirmed by fluorescence microscopy. Figure 6a-b shows large crystals (> 20 μm) with the characteristic well-defined hexagonal and elongated AFI-like phase particles, which are intergrown with rectangular plate-like AEL particles. AFI crystals are not fluorescent, whereas AEL crystals display high and homogeneously distributed fluorescence. Furthermore, the channels of MgAPO-AEL ensure a preferred alignment of the organic dye molecules along the pores, as observed through fluorescence microscopy, where large dichroic ratios (D values of around 30-40) were determined for the 4-DASPI@MgAPO-AEL single particles (Figure 6c-d).

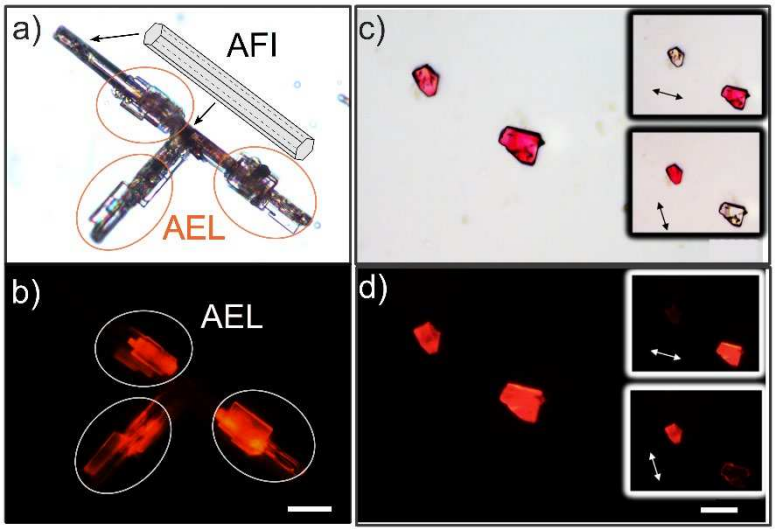

Figure 6. (a-c) Transmission and fluorescence (c-d) images under green light excitation (HQ530/30m bandpass) taken for sample 4-DASPI@MgAPO-AEL-1 (left) and 4-DASPI@MgAPOAEL-6 (right). Note: an illustrative scheme of AFI –type crystals is included in the transmission image. Polarized transmission and fluorescence images are inset (arrows indicate the direction of the polarized light); scale bar = 20 μm.

Overall, 4-DASPI@MgAPO-AEL samples show an emission band centered at around 610.0 nm, which is slightly blue-shifted with respect to solution (618.5 nm). The lower blue-shift registered with respect to that found in the fluorescence band for 4-DASPI@MgAPO-CHA (583.0 nm) could point to a less tighter confinement reached in the latter framework. However, the higher emission efficiency (ϕ_{fl} = 41%) and longer lifetimes recorded for 4-DASPI@MgAPO-AEL-6 (τ = 3.3 ns) with respect to 4-DASPI@MgAPO-CHA (2.7 ns) indicates the opposite, since larger fluorescence quantum yields and lifetimes are a consequence of a reduction of non-radiative processes as a result of higher molecular movement restriction (supported later in section 3E). Hence, the observed variations in the emission band positions for 4-DASPI into AEL and CHA can be attributed to two possible factors: i) distinct geometries of the excited state charge transfer (CT) state, as depicted in Figure 7. The dye molecule's conformation within CHA pores shows a larger deviation from planarity (Figure 7a) compared to the simulation within AEL (Figure 7b), which leads to a larger blue-shift and a less energy stabilized CT state [39]; and ii) the inner filter effect, wherein the greater dye uptake and higher overlap between absorption and emission bands in 4-DASPI@MgAPO-AEL samples (Figure S4 and S5) contribute to a red-shift in emission. Thus, the AEL matrix seems to impose a higher restriction on dye molecules, decreasing more efficiently non-radiative pathways.

Note here that for sample 4-DASPI@MgAPO-AEL-1, the lower fluorescence quantum yield and the biexponential behavior observed in the fluorescence decay curves is likely once again attributed to the presence of AFI impurities. This results in a less emissive system and, consequently, shorter lifetime values. Hence, the longest lifetime of about 3 ns with a weight of 80% is ascribed to 4-DASPI dye within the AEL structure, while the shortest lifetime of about 0.13 ns with a weight of 20% indicates a less rigid environment, which is likely due to 4-DASPI within the AFI structure.

 doi:10.20944/preprints202402.0625.v1

In summary, the photophysics of the 4-DASPI dye, in particular the emission efficiency and lifetimes, have been improved with respect to 4-DASPI in solution by the encapsulation of these dye molecules within cavities and channels of CHA and AEL zeolitic structures, respectively, with only the latter displaying a preferential orientation of dyes. Nevertheless, the confinement seems to be better in the AEL framework. Besides, these samples have a higher dye loading and a preferential orientation of the dye molecules along 1D-channels, which could potentially trigger intriguing NLO optical properties such as SHG. Further experiments are planned to explore optical properties such as second-harmonic generation (SHG) and laser action. For that, additional synthesis will be conducted to attain particles with suitable size, shape and dye loading.

3.E. Molecular Simulations

We finally analyzed the confinement of 4-DASPI dyes (MC state, which is predominant) within the two frameworks by molecular simulations (based on the cvff forcefield). Figure 7 displays the most stable configuration for the MC species of 4-DASPI dye in CHA (a) and AEL (b) frameworks, where energy results indicate a much higher stability (more negative interaction energy, I.E.) for 4-DASPI within the AEL framework (-94.0 compared to -52.9 for CHA), thus explaining the higher incorporation experimentally found in AEL. As for related LDS 722 system, 4-DASPI molecules locate well-aligned within the AEL channels (Figure 7b), showing a very good host-guest fit that imposes a high restriction to motions and deviation from planarity [20]. A different configuration is found for 4-DASPI confined within the CHA framework; cha cavities were found to be not large enough as to host a complete 4-DASPI molecule, and hence molecular simulations suggest that the dye should locate along adjacent cavities, siting the alkenyl intermediate chain within the 8-ring windows that connect the two cavities, and each bulky aromatic group within each cavity (Figure 7a). This type of configuration has been previously found for organic cations acting as structure-directing agents with a similar molecular structure based on bulky aromatic rings linked by alkyl chains [40]. Interestingly, this particular configuration involves that 4-DASPI dye molecules can be oriented in any of the three directions perpendicular to the 8-ring windows connecting the cha cavities, as can be observed in Figure 7a (inset), what explains the lack of a preferential orientation found experimentally.

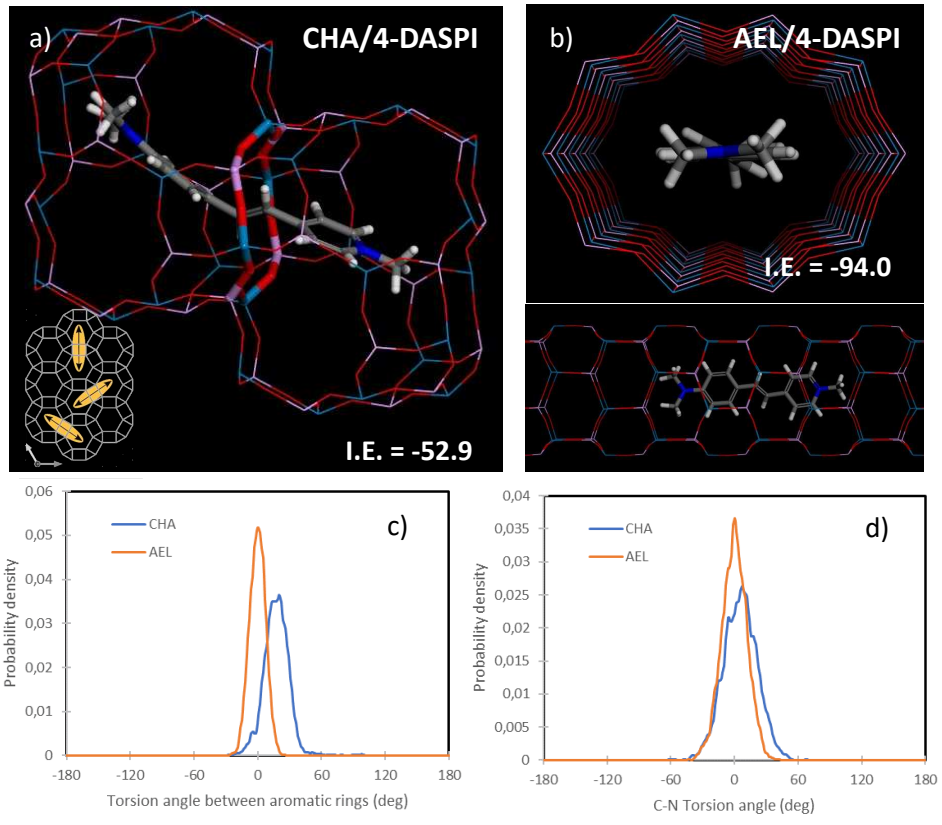

 doi:10.20944/preprints202402.0625.v1

Figure 7. Molecular simulations of 4-DASPI confined within CHA or AEL frameworks. Most stable location within CHA (a) or AEL (b) frameworks, and distribution of torsion angle between the two aromatic rings (c) and of the C-N (aniline) bonds (d).

In order to estimate the restrictions to motion imposed by each framework, 500 ps of MD simulations were run (at 298 K). Deviation from planarity between the two aromatic rings was estimated by plotting the distribution of the torsion angle between the two rings (Figure 7c), while rotation around the aniline C-N bond was estimated by the distribution of the corresponding torsion angle along the MD simulation (Figure 7d). MD results showed a higher restriction to deviation from planarity of the aromatic rings and to rotation of the C-N bond for the AEL framework (estimated as the higher density of probability for torsion angles of 0 deg), hence suggesting that AEL framework imposes a higher confinement and restriction to motion to 4-DASPI, thus explaining the experimental observations of the higher quantum efficiency and longer lifetimes values for AEL. In contrast, for 4-DASPI in the cavity-based CHA framework, siting the intermediate chain within a small 8-ring window would provide a tight confinement to the (poly)methine chain, albeit at the expense of locating the bulky aromatic ring groups within the large cavities that would impose less restriction to motion, resulting in a slightly less restricted confinement, and where dyes do not display a preferential orientation. This can be considered a novel hybrid system with a rather particular dye arrangement, giving rise to distinctive photophysical properties.

4. Materials and Methods

Synthesis of Hybrid Materials

Typical syntheses of MgAPO-CHA involve high temperature of 190 °C [41], which may cause the degradation of the dye. For this reason, we set up a new synthetic protocol at a lower crystallization temperature (150 °C), which involved the addition of a higher amount of TEA as SDA and magnesium. Hence, synthesis of MgAPO-CHA was performed from gels with the following molar composition: 3.3 TEA: 0.47 MgO: 0.765 Al_2O_3: 1 P_2O_5: 0.024 4-DASPI: 47 H_2O. In a typical synthesis procedure, pseudoboehmite (Al_2O_3, Sasol, 75%) was added to a solution of orthophosphoric acid (H_3PO_4, Aldrich, 85%) in water and left stirring for 15 min. Next, triethylamine (TEA, Aldrich, 99.5%,) was added to the solution and stirred for 10 min, followed by the addition of magnesium acetate tetrahydrate ($Mg(acet)_2{\cdot}4\ H_2O$, Aldrich, 99%) and kept for additional 10 min of stirring. Then, 4-DASPI (trans-4-[4-(dimethylamino)styryl]-1-methyl-pyridinium iodide, Aldrich, 98%) was added and kept stirring for 2 h [41]. The gels were introduced into autoclaves to be heated statically in a conventional oven at 150 °C for 48 h.

In the synthesis of 4-DASPI@MgAPO-AEL, the initial molar composition of the gel was: 0.95 Al_2O_3: 1 P_2O_5: x MgO: y EBA: z Dye: 300 H_2O, the same used in our previous works [20]. However, since we found the co-crystallization of the AFI phase as a consequence of the presence of 4-DASPI, we slightly varied x, y and z in order to minimize the presence of such competing phase; details are given in the results section. In a general produce, ortophosphoric acid was mixed with Milli-Q water and kept under vigorous stirring for 2 minutes. Next, magnesium acetate tetrahydrate and aluminum hydroxide ($Al(OH)_3$, Aldrich) were gently added and the resulting mixture was left under stirring for 10 minutes. Ethyl-butylamine was then added to the reaction gel together with the organic dye and was kept stirring for 1 h. The aqueous mixture was then heated statically at 180 °C in an autoclave for 24 hours in a conventional oven. All solid products were recovered by filtration, exhaustively washed with ethanol and water, and dried at room temperature overnight.

Characterization Techniques

X-Ray powder diffraction (PXRD) was used to identify the crystalline framework structures of the solids. The diffraction patterns were collected by using a Philips X'pert PRO automatic diffractometer with Cu-Kα radiation (λ = 1.5418 Å) and a PIXcel solid-state detector). The size and morphology of the samples were characterized by SEM in a JEOL JSM-6400 (tungsten filament)

 doi:10.20944/preprints202402.0625.v1

operating at 20 kV and 10^{-11} A. These measurements were carried out at the University of the Basque Country UPV-EHU, SGIker facilities.

Quantification of DASPI Loading into MgCHA and MgAEL

The final dye loadings incorporated into the aluminophosphate powders were quantified spectrometrically after dissolving a certain amount (10 mg) of the sample powder in hydrochloric acid (5 M). The absorption spectra of the samples were compared with the absorptions of the previously prepared standard solutions (with known concentrations), making a calibration curve at analogous conditions. The absorption spectra were recorded with a UV-Vis spectrophotometer (Cary 7000) described below. Dye content values are given throughout this work as mmol of dye per 100 g sample powder and in percentage with respect to the initial amount added in the synthesis gel.

Photophysical Characterization

Absorption spectra were recorded in a double beam Agilent Cary 7000 universal measurement spectrophotometer (UMS) with a Hamamatsu R928 photomultiplier as a detector, in transmittance for solutions (organic dye, standards and dye-loading quantification), by baseline correction, and with an integrating sphere for bulk powder (Internal DRA 900). Steady-state fluorescence measurements were carried out in an Edinburgh Instruments Spectrofluorimeter (FLSP920 model), with a photomultichannel tube, PMT (Hamamatsu R2658P) as a detector. Fluorescence quantum yields were determined via absolute method, through an integrating sphere in the same spectrofluorimeter. Fluorescence microscopy images were recorded with an optical upright wide-field microscope with epi configuration (Olympus BX51) equipped with a color CCD camera (DP72) using HQ530/30m band pass, Q660LP dichroic filter and E580lp cut-off. Dichroic ratio D, generally defined as the ratio between the intensities recorded for orthogonal emission polarizations, is determined as an indicative parameter of molecule orientation within the pores as: $D = I_{\parallel} / I_{\perp}$, where $I_{\parallel}$ and $I_{\perp}$ are the fluorescence intensities measured with the analyzer parallel and perpendicular to the sample crystal axis, respectively.

Computational Details

Ground state (S_0) geometries of isolated 4-DASPI were optimized by Density Functional Theory (DFT) using the B3LYP hybrid functional and the triple valence basis set with one polarization function (6-311g*) [42,43]. The geometries were checked by frequency analysis to know whether it corresponded to a true energy minimum and this was confirmed when the analysis did not give any negative value. From the optimized geometries, the molecular dipole moments of the organic dyes and the molecular orbitals HOMO (Highest Occupied Molecular Orbital) and LUMO (Lowest Unoccupied Molecular Orbital) were determined. All the simulations were conducted at the Gaussian 16 software in the computational cluster ARINA of the University of the Basque Country UPV-EHU.

Calculations on the location of dyes embedded within the CHA and AEL framework structures were based on molecular mechanics, as implemented in Forcite module, in Materials Studio software (Material Studio 2022, BIOVIA). Molecular mechanics calculations were based on the cvff forcefield [39,44]. The most stable location of DASPI cations within the two frameworks was obtained by first loading one dye molecule by Monte-Carlo simulations (Sorption module with fixed loading at 1), and then obtaining the most stable configuration by simulated annealing calculations. NVT Molecular Dynamics simulations (Forcite module) were run at 298 K in order to analyze the motion of 4-DASPI within the two frameworks, calculating the torsion angle distribution along the MD simulations.

5. Conclusions

By employing various magnesium-doped aluminophosphates (AEL and CHA) to provide a rigid environment for hosting 4-DASPI dye molecules, fluorescence quantum yields and excited-state lifetimes have been significantly increased by slowing down the torsional motion of the dye. The different inorganic matrices influence and modulate the photophysical properties of this fluorophore

 doi:10.20944/preprints202402.0625.v1

offering different functionalities to the resulting hybrid material. Thus, depending on the type of framework system, based on channels or cavities, highly fluorescent systems either with a preferential dye alignment or smaller crystals with isotropic response have been obtained for potential applications such as SHG (Second Harmonic Generation) or laser action devices, respectively. The novel design of Dye@MgAPO-CHA system, in which dye molecules are hosted sharing large cavities connected by smaller windows, opens up new possibilities to explore other hybrid systems, which are likely to provide new optical functionalities.

Supplementary Materials: The following supporting information can be downloaded at: www.mdpi.com/xxx/s1, Figure S1: a) Height-normalized absorption and emission spectra (λ_{exc} = 420 nm) recorded for the 4-DASPI dye in aqueous solution; b) HOMO-LUMO orbitals of 4-DASPI dye; Figure S2: Equilibrium between monocation (MC) and dication (DC) species of 4-DASPI dye in aqueous solution; Figure S3: Photographs of samples 4-DASPI@MgAPO-AEL (1) and (6) in powder under ambient and UV light; Figure S4 and Figure S5: Absorption, excitation and emission (λ_{exc} = 500 nm) spectra of sample 4-DASPI@MgAPO-AEL-1 and 4-DASPI@MgAPO-AEL-6, respectively).

Author Contributions: Conceptualization, L.G.H. and V.M.M..; investigation, A.O.S., R.S.L., L.G.H. and V.M.M.; resources, J.P.P., L.G.H. and V.M.M. writing—original draft preparation, A.O.S., L.G.H. and V.M.M.; writing—review and editing,. A.O.S, J.P.P., L.G.H., R.S.L. and V.M.M; supervision, L.G.H. and V.M.M.; project administration, J.P.P., L.G.H. and V.M.M.; funding acquisition, J.P.P., L.G.H. and V.M.M.

Funding: This work has been partially financed by the Spanish State Research Agency (Agencia Española de Investigación, AEI, MCIN/AEI/10.13039/501100011033, through projects PID2020-114347RB-C32, PID2019-107968RB-I00 and PID2022-138481NB-I00), Gobierno Vasco - Eusko Jaurlaritza (project IT1639-22) and the European Regional Development Fund (Fondo Europeo de Desarrollo Regional, FEDER).

Acknowledgments: In this section, you can acknowledge any support given which is not covered by the author contribution or funding sections. This may include administrative and technical support, or donations in kind (e.g., materials used for experiments).

Conflicts of Interest: The authors declare no conflicts of interest

References

1. Wuskell, J.P.; Boudreau, D.; Wei, M. De; Jin, L.; Engl, R.; Chebolu, R.; Bullen, A.; Hoffacker, K.D.; Kerimo, J.; Cohen, L.B.; et al. Synthesis, Spectra, Delivery and Potentiometric Responses of New Styryl Dyes with Extended Spectral Ranges. *J Neurosci Methods* **2006**, *151*, 200–215, doi:10.1016/j.jneumeth.2005.07.013.
2. Safir Filho, M.; Fiorucci, S.; Martin, A.R.; Benhida, R. Design, Synthesis and Photophysical Studies of Styryl-Based Push--Pull Fluorophores with Remarkable Solvatofluorochromism. *New Journal of Chemistry* **2017**, *41*, 13760–13772.
3. Du, Y.; Liu, X.; Zhu, S. Near-Infrared-II Cyanine/Polymethine Dyes, Current State and Perspective. *Front Chem* **2021**, *9*.
4. Kothavale, S.; Sekar, N. Methoxy Supported, Deep Red Emitting Mono, Bis and Tris Triphenylamine-Isophorone Based Styryl Colorants: Synthesis, Photophysical Properties, ICT, TICT Emission and Viscosity Sensitivity. *Dyes and Pigments* **2017**, *136*, 116–130.
5. Abeywickrama, C.S.; Wijesinghe, K.J.; Stahelin, R. V; Pang, Y. Bright Red-Emitting Highly Reliable Styryl Probe with Large Stokes Shift for Visualizing Mitochondria in Live Cells under Wash-Free Conditions. *Sens Actuators B Chem* **2019**, *285*, 76–83.
6. Dahal, D.; Ojha, K.R.; Pokhrel, S.; Paruchuri, S.; Konopka, M.; Liu, Q.; Pang, Y. NIR-Emitting Styryl Dyes with Large Stokes' Shifts for Imaging Application: From Cellular Plasma Membrane, Mitochondria to Zebrafish Neuromast. *Dyes and Pigments* **2021**, *194*, 109629.
7. Li, B.; Tong, R.; Zhu, R.; Meng, F.; Tian, H.; Qian, S. The Ultrafast Dynamics and Nonlinear Optical Properties of Tribranched Styryl Derivatives Based on 1, 3, 5-Triazine. *J Phys Chem B* **2005**, *109*, 10705–10710.
8. Huang, J.Y.; Lewis, A.; Loew, L. Nonlinear Optical Properties of Potential Sensitive Styryl Dyes. *Biophys J* **1988**, *53*, 665–670.
9. Millard, A.C.; Jin, L.; Wuskell, J.P.; Lewis, A.; Loew, L.M.; others Sensitivity of Second Harmonic Generation from Styryl Dyes to Transmembrane Potential. *Biophys J* **2004**, *86*, 1169–1176.
10. Supabowornsathit, K.; Faikhruea, K.; Ditmangklo, B.; Jaroenchuensiri, T.; Wongsuwan, S.; Junpra-Ob, S.; Choopara, I.; Palaga, T.; Aonbangkhen, C.; Somboonna, N. Dicationic Styryl Dyes for Colorimetric and Fluorescent Detection of Nucleic Acids. *Sci Rep* **2022**, *12*, 14250.

11. Deligeorgiev, T.; Vasilev, A.; Kaloyanova, S.; Vaquero, J.J. Styryl Dyes - Synthesis and Applications during the Last 15 Years. *Coloration Technology* 2010, *126*, 55–80.
12. Wickramasinghe, N.I.; Corbin, B.; Kanakarathna, D.Y.; Pang, Y.; Abeywickrama, C.S.; Wijesinghe, K.J. Bright NIR-Emitting Styryl Pyridinium Dyes with Large Stokes' Shift for Sensing Applications. *Biosensors (Basel)* **2023**, *13*, 799.
13. Cao, X.; Tolbert, R.W.; McHale, J.L.; Edwards, W.D. Theoretical Study of Solvent Effects on the Intramolecular Charge Transfer of a Hemicyanine Dye. *J Phys Chem A* **1998**, *102*, 2739–2748.
14. Mártire, D.; Massad, W.; Montejano, H.; Gonzalez, M.; Caregnato, P.; Villata, L.; Garc\'\ia, N. Properties of Singlet-and Triplet-Excited States of Hemicyanine Dyes. *Chemical Papers* **2014**, *68*, 1137–1140.
15. Lee, Y.; Lee, M. Volume Increment Effect on the Photoisomerization of Hemicyanine Dyes in Oligo(Ethylene Glycol)s. *Journal of Physical Chemistry A* **2013**, *117*, 12878–12883, doi:10.1021/jp4101043.
16. Schmidtke, J.; Stille, W.; Finkelmann, H.; Kim, S.T. Laser Emission in a Dye Doped Cholesteric Polymer Network. *Advanced materials* **2002**, *14*, 746–749.
17. Xu, B.; Gao, Z.; Wei, Y.; Liu, Y.; Sun, X.; Zhang, W.; Wang, X.; Wang, Z.; Meng, X. Dynamically Wavelength-Tunable Random Lasers Based on Metal–Organic Framework Particles. *Nanoscale* **2020**, *12*, 4833–4838.
18. Udayan, S.; MM, R.S.; Sebastian, M.; Nampoori, V.P.N.; Thomas, S. Two Photon Induced Amplified Spontaneous Emission at Low Threshold from Styryl 7 Dye Incorporated DNA Template. *Opt Mater (Amst)* **2018**, *86*, 492–497.
19. Yu, J.; Cui, Y.; Wu, C.; Yang, Y.; Wang, Z.; O'Keeffe, M.; Chen, B.; Qian, G. Second-Order Nonlinear Optical Activity Induced by Ordered Dipolar Chromophores Confined in the Pores of an Anionic Metal--Organic Framework. *Angewandte Chemie* **2012**, *124*, 10694–10697.
20. Sola-Llano, R.; Martínez-Martínez, V.; Fujita, Y.; Gómez-Hortigüela, L.; Alfayate, A.; Uji-i, H.; Fron, E.; Pérez-Pariente, J.; López-Arbeloa, I. Formation of a Nonlinear Optical Host–Guest Hybrid Material by Tight Confinement of LDS 722 into Aluminophosphate 1D Nanochannels. *Chemistry - A European Journal* **2016**, *22*, 15700–15711, doi:10.1002/chem.201601736.
21. IZA International Zeolite Association Available online: https://europe.iza-structure.org/IZA-SC/ftc_table.php.
22. Sola-Llano, R.; Fujita, Y.; Gómez-Hortigüela, L.; Alfayate, A.; Uji-I, H.; Fron, E.; Toyouchi, S.; Pérez-Pariente, J.; López-Arbeloa, I.; Martínez-Martínez, V. One-Directional Antenna Systems: Energy Transfer from Monomers to J-Aggregates within 1D Nanoporous Aluminophosphates. *ACS Photonics* **2018**, *5*, 151–157, doi:10.1021/acsphotonics.7b00553.
23. Sola-Llano, R.; Gartzia-Rivero, L.; Oliden-Sanchez, A.; Bañuelos, J.; Arbeloa, I.L.; Martínez-Martínez, V. Dye Encapsulation into One-Dimensional Zeolitic Materials for Optical Applications. In *Chemistry of Silica and Zeolite-Based Materials*; Elsevier, 2019; pp. 229–248.
24. Martínez, V.; García Salas, R.; Gómez-Hortigüela Sainz, L.; Pérez Pariente, J.; López-Arbeloa, Í. Modulating Dye Aggregation by Incorporation into 1D-MgAPO Nanochannels. *Chemistry--A European Journal* **2013**, *19*, 9859–9865.
25. Sola-Llano, R.; Oliden-Sánchez, A.; Alfayate, A.; Gómez-Hortigüela, L.; Pérez-Pariente, J.; Arbeloa, T.; Hofkens, J.; Fron, E.; Martínez-Martínez, V. White Light Emission by Simultaneous One Pot Encapsulation of Dyes into One-Dimensional Channelled Aluminophosphate. *Nanomaterials* **2020**, *10*, 1173, doi:10.3390/nano10061173.
26. PetteráLillerud, K.; others Two Members of the ABC-D6R Family of Zeolites: Zeolite Phi and Linde D. *Journal of the Chemical Society, Faraday Transactions* **1994**, *90*, 1547–1551.
27. Turrina, A.; Garcia, R.; Watts, A.E.; Greer, H.F.; Bradley, J.; Zhou, W.; Cox, P.A.; Shannon, M.D.; Mayoral, A.; Casci, J.L.; et al. STA-20: An ABC - 6 Zeotype Structure Prepared by Co-Templating and Solved via a Hypothetical Structure Database and STEM-ADF Imaging. **2017**, doi:10.1021/acs.chemmater.6b04892.
28. Wilson, S.T.; Broach, R.W.; Blackwell, C.S.; Bateman, C.A.; McGuire, N.K.; Kirchner, R.M. Synthesis, Characterization and Structure of SAPO-56, a Member of the ABC Double-Six-Ring Family of Materials with Stacking Sequence AABBCCBB. *Microporous and mesoporous materials* **1999**, *28*, 125–137.
29. McCusker, L.B.; Olson, D.H.; Baerlocher, C. *Atlas of Zeolite Framework Types*; 2007; ISBN 9780444530646.
30. Dent, L.S.; Smith, J. V Crystal Structure of Chabazite, a Molecular Sieve. *Nature* **1958**, *181*, 1794–1796.
31. Saxton, C.G.; Kruth, A.; Castro, M.; Wright, P.A.; Howe, R.F. Xenon Adsorption in Synthetic Chabazite Zeolites. *Microporous and mesoporous materials* **2010**, *129*, 68–73.
32. García Salas, R.; Pérez Pariente, J.; Gómez Hortigüela, L.; Martínez Martínez, V.; López Arbeloa, I. Hybrid Photoactive Material, Method for Obtaining Same and Use of the Material 2014.
33. Chen, Y.; Fu, L.; Xu, X.; Ling Li, I.; Ruan, S.; Jian, D.; Zhai, J. Host-Guest Interaction between Acridine Orange Molecules and AFI or CHA Zeolite Crystals., doi:10.1117/12.2257879.
34. Hoppe, R.; Schulz-Ekloff, G.; Wöhrle, D.; Shpiro, E.S.; Tkachenko, O.P. Xps Investigation of Methylene Blue Incorporated into Faujasites and AlPO Family Molecular Sieves. *Zeolites* **1993**, *13*, 222–228.

35. Martínez-Martínez, V.; García, R.; Gómez-Hortigüela, L.; Sola Llano, R.; Pérez-Pariente, J.; López-Arbeloa, I. Highly Luminescent and Optically Switchable Hybrid Material by One-Pot Encapsulation of Dyes into MgAPO-11 Unidirectional Nanopores. *ACS Photonics* **2014**, *1*, 205–211, doi:10.1021/ph4000604.
36. Jee, A.Y.; Bae, E.; Lee, M. Internal Motion of an Electronically Excited Molecule in Viscoelastic Media. *Journal of Chemical Physics* **2010**, *133*, doi:10.1063/1.3454724.
37. Jee, A.Y.; Lee, M. Excited-State Dynamics of a Hemicyanine Dye in Polymer Blends. *ChemPhysChem* **2010**, *11*, 793–795, doi:10.1002/cphc.200900819.
38. Zhang, Z.; Zhang, G.; Wang, J.; Sun, S.; Zhang, Z. The Mechanisms of Large Stokes Shift and Fluorescence Quantum Yields in Anilino Substituted Rhodamine Analogue: TICT and PICT. *Comput Theor Chem* **2016**, *1095*, 44–53.
39. Brunel, D.; Dumur, F. Recent Advances in Organic Dyes and Fluorophores Comprising a 1, 2, 3-Triazole Moiety. *New Journal of Chemistry* **2020**, *44*, 3546–3561.
40. Tavares, T.K.; Almeida, G.; Variani, Y.M.; Bernardo-Gusmao, K.; Vinaches, P.; Alcântara, A.C.S.; Paiva, A.E.M.; Gómez-Hortigüela, L.; Rojas, A. Structure-Directing Study of 1-Methylimidazolium-Based Dication with Tetramethylene as Spacer Length in the Synthesis of Microporous Silicoaluminophosphates. *New Journal of Chemistry* **2021**, *45*, 7185–7195.
41. Concepción, P.; Nieto, J.M.L.; Mifsud, A.; Pérez-Pariente, J. Preparation and Characterization of Mg-Containing AFI and Chabazite-Type Materials. *Zeolites* **1996**, *16*, 56–64.
42. Krishnan, R.; Binkley, J.S.; Seeger, R.; Pople, J.A. Self-Consistent Molecular Orbital Methods. XX. A Basis Set for Correlated Wave Functions. *J Chem Phys* **1980**, doi:10.1063/1.438955.
43. Frisch, M.J.; Pople, J.A.; Binkley, J.S. Self-Consistent Molecular Orbital Methods 25. Supplementary Functions for Gaussian Basis Sets. *J Chem Phys* **1984**, doi:10.1063/1.447079.
44. Dauber-Osguthorpe, P.; Roberts, V.A.; Osguthorpe, D.J.; Wolff, J.; Genest, M.; Hagler, A.T. Structure and Energetics of Ligand Binding to Proteins: Escherichia Coli Dihydrofolate Reductase-trimethoprim, a Drug-receptor System. *Proteins: Structure, Function, and Bioinformatics* **1988**, *4*, 31–47.